Supporting Information for: Density Functional Theory for Molecule-Metal Surface Reactions: When Does the Generalized Gradient Approximation Get It Right, and What to Do If It Doesn't

Nick Gerrits*[1], Egidius W.F. Smeets[1], Stefan Vuckovic[2], Andrew D. Powell[1], Katharina Doblhoff-Dier[1], and Geert-Jan Kroes†[1]

[1]Leiden Institute of Chemistry, Leiden University, Gorlaeus Laboratories, P.O. Box 9502, 2300 RA Leiden, The Netherlands
[2]Department of Chemistry, University of California, Irvine, CA 92697, USA

*email: n.gerrits@lic.leidenuniv.nl
†email: g.j.kroes@chem.leidenuniv.nl

Contents

List of Figures

List of Tables

S1 Method

S1.1 Density functionals used in this study

The three DFs selected in our study are the RPBE DF (in the sense that its results serve as a yardstick to measure other results against), and the MS-RPBEl[1] and HSE03-1/3X[2–4] DFs used in the study of the dissociative chemisorption of O_2 on Al(111). Here we briefly discuss the choice of these functionals.

The RPBE DF[5] may be viewed as a non-empirical GGA functional just like the PBE DF[6], as Hammer et al. made sure that the constraints imposed on the PBE DF are also imposed on the RPBE-DF[6,7]. This includes the recovery of the uniform electron gas (UEG) limit, which ensures the functional's applicability to metals[8]. The RPBE DF, which was originally designed to improve the chemisorption energies of atoms and molecules on metals, which are severely overestimated with PBE, yields higher barriers for gas phase reaction barriers than PBE, thereby improving on their description (e.g. the mean unsigned error for the barrier heights in the HTBH38/08 and NHTBH38/08 databases is reduced from 8.9 to 6.6 kcal/mol going from PBE to RPBE). The RPBE DF also yields consistently higher barriers for dissociative chemisorption reactions on metals[9,10] than the PBE DF and, in fact, than any non-empirical GGA DF obeying the UEG limit that we know of. Hence, we use RPBE[5] (or RPBE-vdW-DF1[5,11]) results as yardstick to measure other results for dissociative chemisorption systems against: if the RPBE (RPBE-vdW-DF1) DF yields a barrier that is too low, perhaps a meta-GGA but probably a hybrid DF will have to be used to obtain a higher barrier.

Some important advantages of the MS-RPBEl meta-GGA DF tested on O_2 + Al(111) have already been mentioned in the main paper. They include an approximate correction for one electron-self interaction, which is ensured by demanding that the functional reproduce the energy of the H-atom and the atomic/molecular orbital limit. Based on this approximate correction one might expect the functional to perform well on reaction barrier heights, the description of which may suffer from self-interaction errors[12–14]. The MS-RPBEl DF gives a chemically accurate description of the dissociative chemisorption of H_2 on Cu(111), and also a quite accurate description of that of H_2 on Ag(111)[1], which are additional reasons for including it here. The performance of this MS functional is in contrast to that of the meta-GGA MS2 DF[15], which, although based on similar design principles, with a mean signed error of -7.8 kcal/mol showed a rather poor performance on the dissociative chemisorption barriers in the SBH10 database[16].

The hybrid DF HSE03-1/3X that we applied to O_2 + Al(111) may be viewed as a re-parameterized version of HSE06[4]. HSE06 is a screened hybrid DF with an exact exchange ratio α equal to 0.25 as in the PBE0 DF[17,18]; at very short range it equals PBE0 and at long range the PBE DF is obtained. As originally intended[2], the HSE03 DF (which at the start suffered from an implementation error[3]) is the

HSE06 DF with a slightly different range parameter ($0.15\,\mathrm{bohr}^{-1}$)[2] than used in HSE06 ($0.11\,\mathrm{bohr}^{-1}$)[4]. However, the most important change made going from HSE06 to HSE03-1/3X is that we used a higher exact exchange ratio (1/3) than the value implemented originally in HSE06 and PBE0 (0.25). Increasing the ratio of exact exchange in a hybrid DF is a longstanding[19–21] and accepted[22,23] practice for improving its performance on gas phase reaction barrier heights. For example, the M08-SO and MOX-HX DFs[21] have $\alpha = 0.57$ and 0.52, respectively, and are among the best three performing functionals for the BH206 database[22]. An example that is pertinent to using HSE03-1/3X instead of HSE03, as done here, showed that changing α from 1/4 to 1/3 in PBE0 reduces the mean absolute error in the reaction barrier heights of the DBH24/08 database from 4.0 to 2.9 kcal/mol[24]. A more minor change we made to HSE06 mentioned already above is that we used a somewhat larger value for the screening parameter, i.e., the one corresponding to HSE03. Note that with the recommended VASP settings (screening parameters of $0.2\,\text{Å}^{-1}$ ($\approx 0.106\,\mathrm{bohr}^{-1}$) and $0.3\,\text{Å}^{-1}$ ($\approx 0.159\,\mathrm{bohr}^{-1}$)) the settings we use for HSE03 and HSE06 are actually a bit different than the ones in the original papers (0.11 and $0.15\,\mathrm{bohr}^{-1}$ for HSE06 and HSE03, respectively), but this slight difference should not affect the results much.

S1.2 DFT calculations

The slabs are constructed with the ideal DFT lattice constants obtained for the tested functionals (4.045 and 4.022 Å for the MS-RPBEl and HSE03-1/3X DFs, respectively), which has been obtained from bulk calculation. The computed bulk lattice constants are in excellent agreement with the experimental value of 4.032 Å[25]. Furthermore, all interlayer distances have been optimized, yielding an outer layer expansion of 1.4% for the HSE03-1/3X DF (i.e., the HSE03 DF, but with the fraction of exact exchange equal to 1/3 instead of 1/4) and 1.1% for the MS-RPBEl DF, which is in reasonable agreement with the experimental value of 2.2%[26]. Calculations employing the HSE03-1/3X DF are started from converged spin polarized calculations employing the RPBE DF and then iterated until convergence. Using 2 octa-core Intel E5-2630v3 cpus (i.e., a total of 16 cores), single-point calculations for the O_2 + Al(111) PES take 2 - 6 hours or 1.5 - 5 days for the MS-RPBEl and HSE03-1/3X DFs, respectively. Non-self-consistent single-point calculations employing the HSE03-1/3X DF on the self-consistent electron density yielded by RPBE take 1 - 2 hours.

S1.3 Application of the corrugation reducing procedure (CRP)

The PES is constructed with the CRP[27] with the same set-up of geometries sampled as in Ref.[10], except that the r_{O_2} and Z_{O_2} grids are non-equidistant in order to increase the accuracy near the barrier. For the MS-RPBEl DF r_{O_2} =[0.9, 1.0, 1.1, 1.15, 1.2, 1.225, 1.25, 1.275, 1.3, 1.35, 1.4, 1.5, 1.6, 1.7, 1.8]

Å and Z_{O_2} =[0.25, 0.75, 1.00, 1.25, 1.50, 1.75, 2.0, 2.25, 2.50, 2.75, 3.00, 3.25, 3.50, 4.00, 4.50] Å are employed. Likewise, for the HSE03-1/3X DF r_{O_2} =[1.0, 1.1, 1.15, 1.175, 1.2, 1.225, 1.25, 1.3, 1.4, 1.5, 1.6] Å and Z_{O_2} =[1.00, 1.50, 2.00, 2.25, 2.50, 2.75, 3.00, 3.25, 3.50] Å are employed. We checked that the maximum value of r_{O_2} used does not negatively impact the evaluation of the sticking probability (S_0, see also Section S1.4 below), so that we can accurately describe the dissociation of O_2 on Al(111). Furthermore, the atomic 3D PES for the HSE03-1/3X DF is taken from the MS-RPBEl DF, i.e., it is computed with the MS-RPBEl DF instead of the HSE03-1/3X DF. This does not affect the accuracy of the interpolation as the 3D potential is merely required to reduce the corrugation of the molecular 6D PES (i.e., to ensure that the curvature of the resulting 6D interpolation function is low), and therefore results should not be affected by the choice of the 3D potential as long as it is physically reasonable.

S1.4 Quasi-classical trajectory (QCT) calculations

For the MD simulations a sufficient number of trajectories (at least 1500) are run in order to obtain standard error bars that are smaller than 0.01 (one percentage point). The oxygen molecule is initially placed halfway between the two periodic images of the slab, with the azimuthal and polar angles sampled according to the rotational state[28]. Trajectories are considered to be reacted when the O_2 bond is extended beyond 1.59 Å for the HSE03-1/3X DF or 1.79 Å for the MS-RPBEl DF. Lowering the dissociation criterium for the MS-RPBEl DF from 1.79 Å to 1.59 Å does not affect S_0. When the distance between the molecule and the surface is larger than the initial value (7.5 Å for MS-RPBEl and 5 Å for HSE03-1/3X) and the velocity vector is pointing away from the surface, the trajectory is considered to be scattered. With the employed propagation time of 10 ps each trajectory ends with one of these two outcomes (i.e., trapping at the surface does not lead to ambiguous outcomes). Furthermore, the equations of motion are integrated with the Stoer and Bulirsch method, using a variable time step[29,30]. In using the QCT method, we make the usual assumption that the dynamics calculations are not affected by problems related to zero-point energy conversion or the neglect of other quantum effects like tunneling. These assumptions have also been made in previous dynamics studies of the O_2 + Al(111) reaction[31,32]. Quantum and quasi-classical studies of the CH_4 + Pt(111) system[33] suggest that these conditions should be met in QCT calculations of sticking probabilities exceeding 0.01, where sticking usually proceeds in a classical, over the barrier fashion.

S1.5 Work function and electron affinity values

Our choice of how to compute the difference of the work function and the electron affinity ($W - E_{ea}$) has been a pragmatic one. We have mostly taken the W-values from Table 1 from Ref.[34], which gives

recommended values for a number of metal surfaces based on an evaluation of experimental results, so we use empirical values (see Table S1). The electron affinities have been mostly taken from a NIST database (Ref.[35]) using semi-empirical composite theory with the G4 basis set (see also Table S2). Note that the electron affinity of CH_4 is obtained by taking the difference between the exciplex state ($-40.240\,409$ Hartree (-1094.9978 eV), see Table S3 of Ref.[36]) and ground state ($-40.451\,691$ Hartree (-1100.7471 eV), see Table S2 of Ref.[36]) energies obtained with CCSD(T)/aug-cc-pVQZ.

Of course, one might also want to use an all-DFT approach. Results of Perdew and co-workers[37] suggest that metal surface work functions can be computed with a mean absolute error of 0.16, 0.21, 0.11, 0.11, and 0.08 eV using the LDA[38,39], PBE[6], PBEsol[40], SCAN[41], and SCAN+rVV10[42] DFs, respectively. Furthermore W-values computed for a large range of metal surfaces with DFT have been tabulated for the LDA, the PBE, and the RPBE[5] DFs in the supporting information of Ref.[43].

The calculation of electron affinities of small molecules is not so straightforward[36,44,45], and this is also true for DFT[45,46]. This is especially true if the electron affinity is negative, which means that the anion is unstable with respect to the dissociation into the neutral molecule and a free electron, as the calculation of a metastable state state is required (see e.g. the calculation of the electron affinity of CH_4[36]). As can be seen from Table S2, this is true for all but one (O_2) of the molecules in the molecule-surface systems considered here. Studies that perform benchmarks on the thermochemistry of large numbers of DFs[22,47] typically employ databases containing back corrected experimental electron affinities (G21EA)[45] or electron affinities computed with a high-level ab initio electronic structure method (EA13/03)[47], which exclusively or predominantly contain positive electron affinities of atoms and small molecules only. Given how complicated it is to compute negative electron affinities, we recommend simply using the results from Ref.[35] as obtained using semi-empirical composite theory with the G4 basis set (see Table S2), for reasons discussed in Ref.[36].

S2 Results

S2.1 Self-consistent DFT results for O_2 + Al(111)

Elbow plots (i.e., two-dimensional cuts through the PES for a particular impact site and orientation) are shown for O_2 on Al(111) for the second parallel orientation at the fcc site as obtained with the MS-RPBEl and HSE03-1/3X DFs in Figures S1 and S2, respectively. The configuration mentioned (i.e., the combination of impact site and orientation) corresponds to the minimum barrier geometry found among the configurations studied for the ECW PES, see also Table 2). The two elbow plots are very similar, with the main difference being the height of the barrier and its location (i.e., the value of Z_{O_2},

see also Table 2).

An one-dimensional cut through the HSE03-1/3X PES along the molecule-surface distance is shown in Figure 3 for the fcc //3 configuration and $r = 1.25\,\text{Å}$, for which the barrier height is 12.3 kJ/mol (see Table 2). The barrier is found at $Z = 2.6\,\text{Å}$. For this configuration and r-value, the total magnetic moment (i.e., the number of unpaired electrons) of the O_2 + Al(111) system as a function of Z for $r = 1.25\,\text{Å}$ and the fcc //3 orientation is shown in Figure S3. The magnetic moment is an indicator of charge transfer in the sense that a spin-flip and concomitant change in magnetic moment can only take place after charge transfer from the surface to the molecule has occured[48]. Here it can be seen that when a DF is employed that (roughly) corrects for the SIE (i.e., HSE03-1/3X), the magnetic moment drops more gradually when approaching the surface than with the standard RPBE DF. Previously, this effect has also been shown for the charge of O_2 approaching an Al_5 cluster using (screened) hybrid DFs[49]. Furthermore, from visual inspection it is observed that the charge density is more localized on the O_2 molecule when employing SIE-correcting DFs than when using the RPBE DF (results not shown here).

We have also investigated how the barrier height for O_2 + Al(111) depends on the parameters of the HSE functional we used. As Table S3 shows, the barrier height is rather insensitive to changing the screening parameter (i.e., using HSE03-1/3X rather than HSE06-1/3X changes the barrier height by just 0.4 kJ/mol), while increasing α from 1/4 to 1/3 to 1/2 leads to clear increases in the barrier height, as one would expect from the discussion in Section S1.1. Increasing the exact exchange ratio also decreases the lattice constant of Al somewhat, while the lattice constant is not much affected by changing the screening length parameter (Table S3).

S2.2 Non-self-consistent DFT results for O_2 + Al(111), HCl + Au(111), and NH_3 + Ru(0001)

The barrier heights yielded by non-self-consistent calculations employing a self-consistent density from a different DF, as described in Ref.[50,51], are shown in Table S6. Interestingly, the non-self-consistent calculations yield similar barrier energies as the self-consistent calculations (see also Figure 3). As discussed in the main paper, this implies that even when a different electron density is employed, the relative energy does not change considerably; i.e., the failure of RPBE in yielding an adiabatic barrier for O_2 + Al(111) is not caused by a density-driven error but by a functional error. Only when the molecule is closer to the surface (i.e., the value of Z is lower) does the density driven error play a considerable role. Interestingly, the appearance of the density driven error (see Figure 3) coincides with the increasing difference of the magnetic moment between HSE03-1/3X and RPBE (see Figure S3).

Non-self-consistent calculations of the same kind have also been performed for HCl + Au(111) and

NH_3 + Ru(0001) (see Table S7). In general, increasing the fraction of exact exchange, and therefore diminishing the amount of semi-local PBE exchange, leads to barrier heights higher than those found with PBE. These results suggest that employing range-separated hybrid DFs to systems where $(W - E_{\mathrm{ea}}) < 7\,\mathrm{eV}$ may improve the comparison between theory and experiment compared to that obtained with GGA DFs. The barrier for NH_3 + Ru(0001) obtained with non-self consistent HSE calculations was not yet higher than the previous RPBE-vdW-DF1 result (Table S7), but this will probably change if a screened hybrid function is used that employs semi-local RPBE exchange instead of PBE exchange. The barrier obtained with the HSE03@RPBE-vdW-DF1 approach for HCl + Au(111) were higher than those obtained with any semi-local exchange functional thus far (see Table 4 of Ref.[52], the highest barrier (101.3 kJ/mol) thus far was obtained with RPBE), which should help to get better agreement between theory and experiment for this system.

S2.3 Correlation between $(W - E_{\mathbf{ea}})$ and charge transfer at the TS

The excess charge at the molecule for the TS of several molecule-metal surface systems (i.e., the charge transferred from the metal surface to the molecule) is shown in Table S8. The results show a clear correlation between the amount of charge transferred to the molecule and the difference between the work function and the electron affinity; i.e., when $W - E_{\mathrm{ea}}$ decreases, the amount of excess charge on the molecule increases. One might then also argue that the barriers of the difficult systems should be too low because the difficult systems are affected by charge transfer at the barrier, as semi-local functionals may severely overestimate the interaction of charge transfer complexes[12].

S2.4 Dynamics: Dependence of S_0 on molecular beam conditions

The sticking probability in Figure 1 is obtained for a simulated mono-energetic molecular beam. Simulation of only a single energy instead of a velocity distribution does not affect results considerably for weakly activated systems[53]. The rovibrational state population is sampled according to a Boltzmann-like distribution (see for example Ref.[52]), where it is assumed that the vibrational temperature (T_{vib}) = 300 K and the rotational temperature (T_{rot}) = 9 K, as should be appropriate[54] for supersonic molecular beams containing O_2 and using a room temperature nozzle[55]. Simulating only the rotational ground state of O_2 instead of the distribution according to T_{rot} should lead to a too high sticking probability (this is true even for a rotationally cold beam, see Figure S4), as is also confirmed by experiment[56]. Moreover, even though $T_{\mathrm{vib}} = 300\,\mathrm{K}$ is simulated, the population of the vibrational excited states is negligible (0.1%), and therefore the results for the simulated molecular beam can be considered to be for O_2 in the vibrational ground state. Since the previous results obtained with the flexible periodic

London-Eyring-Polanyi-Sato (FPLEPS) potential energy surface (PES) based on ECW data are for O_2 in the rotational ground state[32], the agreement between the reactivity obtained with the ECW method and the experiments may well have been artificially improved for low E_i in this way (see Figure S4).

S2.5 Dynamics: Dependence of S_0 on the alignment of O_2

Figure 2b shows the sticking probabilities of O_2 in the helicopter, random, and perpendicular orientations relative to the surface (see Ref.[32] for explanations of the orientation distributions), as obtained experimentally and with the HSE03-1/3X DF. Note that different incident energy distributions (and, indeed, incidence energies) have been simulated than employed in the experiment as Kurahashi et al. did not publish experimentally determined beam parameters[57], and that the HSE03-1/3X DF yields a sticking probability of unity for $E_i > 25\,\mathrm{kJ/mol}$. Qualitatively the simulations reproduce the experimental alignment trends[57]: The helicopter orientation is the most reactive one, whereas the perpendicular orientation is least reactive. Quantitatively, the differences between the sticking probabilities obtained for different alignments appear smaller in the theory than in the experiment. This observation gives support to the argument that the slope of the sticking probability curve computed with the HSE03-1/3X DF may be too high because the computed anisotropy of the barrier height at the minimum barrier impact site and at other impact sites is too low.

S2.6 Dynamics: Dependence of S_0 on incidence angle

Figure S5 shows the sticking probability of off-normal incident O_2 on Al(111), where the normal incidence energy is computed as

$$E_{\mathrm{normal}} = \cos^2(\theta) E_i. \tag{S1}$$

Experimental trends in the sticking probability as a function of incidence angle of O_2 in its helicopter and cartwheel orientations are reproduced (see Figure S5a). Furthermore, normal energy scaling (NES)[58] is observed both experimentally and in this work (Figure S5a), while ECW theory slightly deviates from NES (Figure S5b).

S3 Discussion

S3.1 O_2 + metal systems that are useful benchmark systems for dissociative chemisorption

Systems that are useful as benchmarks for dissociative chemisorption exhibit activated dissociation, so that sticking probabilities measured in molecular beam experiments increase with incidence energy[59]. Ideally, the dissociation is not affected by precursor dynamics, and the dissociative chemisorption probability rises to several tens of percent. Unfortunately, there are few O_2-metal systems exhibiting this simple behavior that we know of. As discussed in a recent review paper[60], many O_2-metal surface systems exhibit precursor dynamics, where O_2 first adsorbs molecularly as a superoxo- and/or peroxo-state, and only then dissociates. This complicates the analysis of the dissociation of O_2 on all group 10 metals (Ni, Pd, and Pt)[60]. While it has been known for some time that DFT with GGA functionals can be used to compute properties of these precursor states in reasonable agreement with experiments and that barriers to dissociation can be computed[61,62], comparison of the latter to experimental values is very difficult, and it is hard to establish the reliability of experimental values of barrier heights, which may differ depending on the technique used and the analysis of the experiments[60]. Studies of the O_2 + Pt(111) system[63,64] show how difficult it is to extract information on the dissociative chemisorption in this system, which is activated through thermal fluctuations at low surface temperature[64]."

Extracting accurate information on dissociative chemisorption of O_2 on the group 11 metals Ag and Au likewise is extremely difficult. Au surfaces show very high barriers to O_2 dissociation[60]. As discussed by Juaristi and co-workers, the major disagreement now seen in dynamics calculations on dissociative chemisorption of O_2 on Ag(110), Ag(100), and Ag(111) is due to the difficulty on unraveling the contribution the contributions of molecular and dissociative chemisorption to sticking (see Figure 11 of their work)[65].

The only O_2-metal systems we are aware of that obey the following two conditions that (i) the sticking is activated, not precursor-mediated in a major way, and results in dissociative chemisorption with sticking probabilities equal to a few tens of percent, and that (ii) dynamics calculations using the RPBE density functional have been performed are the O_2 + Al(111)[31] example discussed extensively in our paper, O_2 + Cu(111)[66], and O_2 + CuML/Ru(0001)[66]. In all cases, the dynamics calculations using a RPBE PES substantially overestimated the sticking probability. In the calculations on Cu and Cu/Ru surfaces, the effect of surface atom motion and surface temperature was modeled in an approximate manner, using the GLO model[66].

S3.2 Towards an SRP density functional for O_2 + Al(111)

The HSE03-1/3X clearly is not yet an SRP DF for O_2 + Al(111). We base our below suggestions on how a SRP-DF may be developed on the following observations: (i) Compared to the ECW barrier geometries, the HSE03-1/3X geometries are too early, i.e., the barriers occur too far from the surface, and (ii) the narrow slope in the $S_0(E_i)$ curves obtained with standard GGA exchange-correlation DFs for H_2 + Ru(0001), which is also an early barrier system, could be remedied[10] by using correlation functionals approximately describing the attractive van der Waals dispersion interaction[11,67].

We therefore suggest to proceed with the development of an SRP DF for O_2 + Al(111) as follows. First, the correlation DF in HSE03 (or alternatively HSE06), i.e., the PBE correlation DF, can be replaced with a Van der Waals correlation functional, obvious candidates being the vdW DFs developed for hybrids by Hyldgaard and co-workers[68,69]. Alternatively, one could add the TS-vdW correction as used by Tkatchenko and co-workers to the HSE03 functional[70]. This would probably move the barrier geometries closer to the surface when compared to the HSE03-1/3X geometries. In turn, this would also increase the energetic corrugation and the anisotropy of the barrier heights, and lower the barrier heights. While the former change would probably result in better agreement with experiment for the steepness and the alignment dependence of $S_0(E_i)$ (Figures 2a and 2b, respectively), the energetic threshold of $S_0(E_i)$ would probably also be decreased, possibly resulting in worse agreement with experiment. However, this can probably be offset by increasing the fraction of exact exchange in HSE03 (see Section S2.1). Alternatively, one might think of replacing (a fraction of) the local PBE exchange[6] in HSE03 with RPBE exchange[5]. Finally, a range-separated meta-GGA hybrid DF might perform better[71] than a range-separated GGA hybrid DF. Especially one of the MS kind could perform well, as the MS-RPBEl DF already has shown to improve results for O_2 + Al(111) compared to the RPBE DF. Furthermore, using screened hybrid DFs where the range-separation parameter is either optimally pre-tuned (or self-consistently during calculations) or constrained to reproduce the energy of a free hydrogen atom could also improve results[72–77]. We expect that the approaches sketched can go a long way towards improving the results for O_2 + Al(111), and developing an SRP DF for this system.

Supporting References

(1) Smeets, E. W. F.; Voss, J.; Kroes, G.-J. Specific Reaction Parameter Density Functional Based on the Meta-Generalized Gradient Approximation: Application to H_2 + Cu(111) and H_2 + Ag(111). *J. Phys. Chem. A* **2019**, *123*, 5395–5406.

(2) Heyd, J.; Scuseria, G. E.; Ernzerhof, M. Hybrid Functionals Based on a Screened Coulomb Potential. *J. Chem. Phys.* **2003**, *118*, 8207–8215.

(3) Heyd, J.; Scuseria, G. E.; Ernzerhof, M. Erratum: "Hybrid Functionals Based on a Screened Coulomb Potential" [J. Chem. Phys. 118, 8207 (2003)]. *J. Chem. Phys.* **2006**, *124*, 219906.

(4) Krukau, A. V.; Vydrov, O. A.; Izmaylov, A. F.; Scuseria, G. E. Influence of the Exchange Screening Parameter on the Performance of Screened Hybrid Functionals. *J. Chem. Phys.* **2006**, *125*, 224106.

(5) Hammer, B.; Hansen, L. B.; Nørskov, J. K. Improved Adsorption Energetics within Density-Functional Theory Using Revised Perdew-Burke-Ernzerhof Functionals. *Phys. Rev. B* **1999**, *59*, 7413–7421.

(6) Perdew, J. P.; Burke, K.; Ernzerhof, M. Generalized Gradient Approximation Made Simple. *Phys. Rev. Lett.* **1996**, *77*, 3865.

(7) Nattino, F.; Migliorini, D.; Kroes, G.-J.; Dombrowski, E.; High, E. A.; Killelea, D. R.; Utz, A. L. Chemically Accurate Simulation of a Polyatomic Molecule-Metal Surface Reaction. *J. Phys. Chem. Lett.* **2016**, *7*, 2402–2406.

(8) Perdew, J. P.; Ruzsinszky, A.; Tao, J.; Staroverov, V. N.; Scuseria, G. E.; Csonka, G. I. Prescription for the Design and Selection of Density Functional Approximations: More Constraint Satisfaction with Fewer Fits. *J. Chem. Phys.* **2005**, *123*, 062201.

(9) Díaz, C.; Pijper, E.; Olsen, R. A.; Busnengo, H. F.; Auerbach, D. J.; Kroes, G. J. Chemically Accurate Simulation of a Prototypical Surface Reaction: H_2 Dissociation on Cu(111). *Science* **2009**, *326*, 832–834.

(10) Wijzenbroek, M.; Kroes, G. J. The Effect of the Exchange-Correlation Functional on H_2 Dissociation on Ru(0001). *J. Chem. Phys.* **2014**, *140*, 084702.

(11) Dion, M.; Rydberg, H.; Schröder, E.; Langreth, D. C.; Lundqvist, B. I. Van Der Waals Density Functional for General Geometries. *Phys. Rev. Lett.* **2004**, *92*, 246401.

(12) Zhang, Y.; Yang, W. A Challenge for Density Functionals: Self-Interaction Error Increases for Systems with a Noninteger Number of Electrons. *J. Chem. Phys.* **1998**, *109*, 2604–2608.

(13) Mori-Sánchez, P.; Cohen, A. J.; Yang, W. Many-Electron Self-Interaction Error in Approximate Density Functionals. *J. Chem. Phys.* **2006**, *125*, 201102.

(14) Cohen, A. J.; Mori-Sánchez, P.; Yang, W. Insights into Current Limitations of Density Functional Theory. *Science* **2008**, *321*, 792–794.

(15) Sun, J.; Xiao, B.; Fang, Y.; Haunschild, R.; Hao, P.; Ruzsinszky, A.; Csonka, G. I.; Scuseria, G. E.; Perdew, J. P. Density Functionals That Recognize Covalent, Metallic, and Weak Bonds. *Phys. Rev. Lett.* **2013**, *111*, 106401.

(16) Mallikarjun Sharada, S.; Bligaard, T.; Luntz, A. C.; Kroes, G.-J.; Nørskov, J. K. SBH10: A Benchmark Database of Barrier Heights on Transition Metal Surfaces. *J. Phys. Chem. C* **2017**, *121*, 19807–19815.

(17) Perdew, J. P.; Ernzerhof, M.; Burke, K. Rationale for Mixing Exact Exchange with Density Functional Approximations. *J. Chem. Phys.* **1996**, *105*, 9982–9985.

(18) Adamo, C.; Barone, V. Toward Reliable Density Functional Methods without Adjustable Parameters: The PBE0 Model. *J. Chem. Phys.* **1999**, *110*, 6158–6170.

(19) Truong, T. N.; Duncan, W. A New Direct Ab Initio Dynamics Method for Calculating Thermal Rate Constants from Density Functional Theory. *J. Chem. Phys.* **1994**, *101*, 7408–7414.

(20) Lynch, B. J.; Fast, P. L.; Harris, M.; Truhlar, D. G. Adiabatic Connection for Kinetics. *J. Phys. Chem. A* **2000**, *104*, 4811–4815.

(21) Zhao, Y.; Truhlar, D. G. Exploring the Limit of Accuracy of the Global Hybrid Meta Density Functional for Main-Group Thermochemistry, Kinetics, and Noncovalent Interactions. *J. Chem. Theory Comput.* **2008**, *4*, 1849–1868.

(22) Mardirossian, N.; Head-Gordon, M. Thirty Years of Density Functional Theory in Computational Chemistry: An Overview and Extensive Assessment of 200 Density Functionals. *Mol. Phys.* **2017**, *115*, 2315–2372.

(23) Cohen, A. J.; Mori-Sánchez, P.; Yang, W. Challenges for Density Functional Theory. *Chem. Rev.* **2012**, *112*, 289–320.

(24) Guido, C. A.; Brémond, E.; Adamo, C.; Cortona, P. Communication: One Third: A New Recipe for the PBE0 Paradigm. *J. Chem. Phys.* **2013**, *138*, 021104.

(25) Haas, P.; Tran, F.; Blaha, P. Calculation of the Lattice Constant of Solids with Semilocal Functionals. *Phys. Rev. B* **2009**, *79*, 085104.

(26) Jona, F.; Sondericker, D.; Marcus, P. M. Al(111) Revisited. *J. Phys. C: Solid State Phys.* **1980**, *13*, L155–L158.

(27) Busnengo, H. F.; Salin, A.; Dong, W. Representation of the 6D Potential Energy Surface for a Diatomic Molecule near a Solid Surface. *J. Chem. Phys.* **2000**, *112*, 7641–7651.

(28) Brink, D.; Satchler, G., *Angular Momentum*, Second; Oxford University Press: 1968.

(29) Bulirsch, R.; Stoer, J. Numerical Treatment of Ordinary Differential Equations by Extrapolation Methods. *Numer. Math.* **1966**, *8*, 1–13.

(30) Stoer, J.; Bulirsch, R. In *Introduction to Numerical Analysis*, Stoer, J., Bulirsch, R., Eds.; Springer: New York, NY, 1980, pp 244–313.

(31) Behler, J.; Reuter, K.; Scheffler, M. Nonadiabatic Effects in the Dissociation of Oxygen Molecules at the Al(111) Surface. *Phys. Rev. B* **2008**, *77*, 115421.

(32) Yin, R.; Zhang, Y.; Libisch, F.; Carter, E. A.; Guo, H.; Jiang, B. Dissociative Chemisorption of O_2 on Al(111): Dynamics on a Correlated Wave-Function-Based Potential Energy Surface. *J. Phys. Chem. Lett.* **2018**, *9*, 3271–3277.

(33) Nattino, F.; Ueta, H.; Chadwick, H.; van Reijzen, M. E.; Beck, R. D.; Jackson, B.; van Hemert, M. C.; Kroes, G.-J. Ab Initio Molecular Dynamics Calculations versus Quantum-State-Resolved Experiments on CHD_3 + Pt(111): New Insights into a Prototypical Gas–Surface Reaction. *J. Phys. Chem. Lett.* **2014**, *5*, 1294–1299.

(34) Derry, G. N.; Kern, M. E.; Worth, E. H. Recommended Values of Clean Metal Surface Work Functions. *J. Vac. Sci. Technol. A* **2015**, *33*, 060801.

(35) Johnson III, R. D. Computational Chemistry Comparison and Benchmark Database, NIST Standard Reference Database 101, 2020.

(36) Ramírez-Solís, A.; Vigué, J.; Hinojosa, G.; Saint-Martin, H. Solving the CH_4^- Riddle: The Fundamental Role of Spin to Explain Metastable Anionic Methane. *Phys. Rev. Lett.* **2020**, *124*, 056001.

(37) Patra, A.; Peng, H.; Sun, J.; Perdew, J. P. Rethinking CO Adsorption on Transition-Metal Surfaces: Effect of Density-Driven Self-Interaction Errors. *Phys. Rev. B* **2019**, *100*, 035442.

(38) Kohn, W.; Sham, L. J. Self-Consistent Equations Including Exchange and Correlation Effects. *Phys. Rev.* **1965**, *140*, A1133–A1138.

(39) Perdew, J. P.; Wang, Y. Accurate and Simple Analytic Representation of the Electron-Gas Correlation Energy. *Phys. Rev. B* **1992**, *45*, 13244–13249.

(40) Perdew, J. P.; Ruzsinszky, A.; Csonka, G. I.; Vydrov, O. A.; Scuseria, G. E.; Constantin, L. A.; Zhou, X.; Burke, K. Restoring the Density-Gradient Expansion for Exchange in Solids and Surfaces. *Phys. Rev. Lett.* **2008**, *100*, 136406.

(41) Sun, J.; Ruzsinszky, A.; Perdew, J. P. Strongly Constrained and Appropriately Normed Semilocal Density Functional. *Phys. Rev. Lett.* **2015**, *115*, 036402.

(42) Peng, H.; Yang, Z.-H.; Perdew, J. P.; Sun, J. Versatile van Der Waals Density Functional Based on a Meta-Generalized Gradient Approximation. *Phys. Rev. X* **2016**, *6*, 041005.

(43) Tran, R.; Li, X.-G.; Montoya, J. H.; Winston, D.; Persson, K. A.; Ong, S. P. Anisotropic Work Function of Elemental Crystals. *Surf. Sci.* **2019**, *687*, 48–55.

(44) Richard, R. M.; Marshall, M. S.; Dolgounitcheva, O.; Ortiz, J. V.; Brédas, J.-L.; Marom, N.; Sherrill, C. D. Accurate Ionization Potentials and Electron Affinities of Acceptor Molecules I. Reference Data at the CCSD(T) Complete Basis Set Limit. *J. Chem. Theory Comput.* **2016**, *12*, 595–604.

(45) Goerigk, L.; Grimme, S. A General Database for Main Group Thermochemistry, Kinetics, and Noncovalent Interactions - Assessment of Common and Reparameterized (Meta-)GGA Density Functionals. *J. Chem. Theory Comput.* **2010**, *6*, 107–126.

(46) Su, N. Q.; Xu, X. Insights into Direct Methods for Predictions of Ionization Potential and Electron Affinity in Density Functional Theory. *J. Phys. Chem. Lett.* **2019**, *10*, 2692–2699.

(47) Peverati, R.; Truhlar, D. G. Quest for a Universal Density Functional: The Accuracy of Density Functionals across a Broad Spectrum of Databases in Chemistry and Physics. *Philos. Trans. R. Soc. A* **2014**, *372*, 20120476.

(48) Libisch, F.; Huang, C.; Liao, P.; Pavone, M.; Carter, E. A. Origin of the Energy Barrier to Chemical Reactions of O_2 on Al(111): Evidence for Charge Transfer, Not Spin Selection. *Phys. Rev. Lett.* **2012**, *109*, 198303.

(49) Livshits, E.; Baer, R.; Kosloff, R. Deleterious Effects of Long-Range Self-Repulsion on the Density Functional Description of O_2 Sticking on Aluminum. *J. Phys. Chem. A* **2009**, *113*, 7521–7527.

(50) Kim, M.-C.; Sim, E.; Burke, K. Understanding and Reducing Errors in Density Functional Calculations. *Phys. Rev. Lett.* **2013**, *111*, 073003.

(51) Vuckovic, S.; Song, S.; Kozlowski, J.; Sim, E.; Burke, K. Density Functional Analysis: The Theory of Density-Corrected DFT. *J. Chem. Theory Comput.* **2019**, *15*, 6636–6646.

(52) Gerrits, N.; Geweke, J.; Smeets, E. W.; Voss, J.; Wodtke, A. M.; Kroes, G.-J. Closing the Gap Between Experiment and Theory: Reactive Scattering of HCl from Au(111). *J. Phys. Chem. C* **2020**, *124*, 15944–15960.

(53) Ghassemi, E. N.; Somers, M. F.; Kroes, G.-J. Assessment of Two Problems of Specific Reaction Parameter Density Functional Theory: Sticking and Diffraction of H_2 on Pt(111). *J. Phys. Chem. C* **2019**, *123*, 10406–10418.

(54) Kuebler, N. A.; Robin, M. B.; Yang, J. J.; Gedanken, A.; Herrick, D. R. Fully Resolved Zeeman Pattern in the Stern-Gerlach Deflection Spectrum of O_2 ($^3\Sigma_g^-$, K=1). *Phys. Rev. A* **1988**, *38*, 737–749.

(55) Österlund, L.; Zorić, I.; Kasemo, B. Dissociative Sticking of O_2 on Al(111). *Phys. Rev. B* **1997**, *55*, 15452–15455.

(56) Binetti, M.; Weiße, O.; Hasselbrink, E.; Katz, G.; Kosloff, R.; Zeiri, Y. The Role of Nonadiabatic Pathways and Molecular Rotations in the Oxygen Abstraction Reaction on the Al(111) Surface. *Chem. Phys. Lett.* **2003**, *373*, 366–371.

(57) Kurahashi, M.; Yamauchi, Y. Steric Effect in O_2 Sticking on Al(111): Preference for Parallel Geometry. *Phys. Rev. Lett.* **2013**, *110*, 246102.

(58) Rettner, C. T.; DeLouise, L. A.; Auerbach, D. J. Effect of Incidence Kinetic Energy and Surface Coverage on the Dissociative Chemisorption of Oxygen on W(110). *J. Chem. Phys.* **1986**, *85*, 1131–1149.

(59) Kroes, G.-J. Toward a Database of Chemically Accurate Barrier Heights for Reactions of Molecules with Metal Surfaces. *J. Phys. Chem. Lett.* **2015**, *6*, 4106–4114.

(60) Montemore, M. M.; van Spronsen, M. A.; Madix, R. J.; Friend, C. M. O_2 Activation by Metal Surfaces: Implications for Bonding and Reactivity on Heterogeneous Catalysts. *Chem. Rev.* **2018**, *118*, 2816–2862.

(61) Eichler, A.; Hafner, J. Molecular Precursors in the Dissociative Adsorption of O_2 on Pt(111). *Phys. Rev. Lett.* **1997**, *79*, 4481–4484.

(62) Eichler, A.; Mittendorfer, F.; Hafner, J. Precursor-Mediated Adsorption of Oxygen on the (111) Surfaces of Platinum-Group Metals. *Phys. Rev. B* **2000**, *62*, 4744–4755.

(63) Sendner, C.; Groß, A. Kinetic Monte Carlo Simulations of the Interaction of Oxygen with Pt(111). *J. Chem. Phys.* **2007**, *127*, 014704.

(64) Zhou, Y.; Zhou, L.; Hu, X.; Xie, D. Dynamics Studies of O_2 Collision on Pt(111) Using a Global Potential Energy Surface. *J. Phys. Chem. C* **2020**, *124*, 10573–10583.

(65) Lončarić, I.; Alducin, M.; Juaristi, J. I.; Novko, D. CO Stretch Vibration Lives Long on Au(111). *J. Phys. Chem. Lett.* **2019**, *10*, 1043–1047.

(66) Ramos, M.; Díaz, C.; Martínez, A. E.; Busnengo, H. F.; Martín, F. Dissociative and Non-Dissociative Adsorption of O_2 on Cu(111) and Cu_{ML}/Ru(0001) Surfaces: Adiabaticity Takes Over. *Phys. Chem. Chem. Phys.* **2017**, *19*, 10217–10221.

(67) Lee, K.; Murray, É. D.; Kong, L.; Lundqvist, B. I.; Langreth, D. C. Higher-Accuracy van Der Waals Density Functional. *Phys. Rev. B* **2010**, *82*, 081101(R).

(68) Berland, K.; Jiao, Y.; Lee, J.-H.; Rangel, T.; Neaton, J. B.; Hyldgaard, P. Assessment of Two Hybrid van Der Waals Density Functionals for Covalent and Non-Covalent Binding of Molecules. *J. Chem. Phys.* **2017**, *146*, 234106.

(69) Jiao, Y.; Schröder, E.; Hyldgaard, P. Extent of Fock-Exchange Mixing for a Hybrid van Der Waals Density Functional? *J. Chem. Phys.* **2018**, *148*, 194115.

(70) Marom, N.; Tkatchenko, A.; Rossi, M.; Gobre, V. V.; Hod, O.; Scheffler, M.; Kronik, L. Dispersion Interactions with Density-Functional Theory: Benchmarking Semiempirical and Interatomic Pairwise Corrected Density Functionals. *J. Chem. Theory Comput.* **2011**, *7*, 3944–3951.

(71) Sun, J.; Haunschild, R.; Xiao, B.; Bulik, I. W.; Scuseria, G. E.; Perdew, J. P. Semilocal and Hybrid Meta-Generalized Gradient Approximations Based on the Understanding of the Kinetic-Energy-Density Dependence. *J. Chem. Phys.* **2013**, *138*, 044113.

(72) Baer, R.; Livshits, E.; Salzner, U. Tuned Range-Separated Hybrids in Density Functional Theory. *Annu. Rev. Phys. Chem.* **2010**, *61*, 85–109.

(73) Refaely-Abramson, S.; Sharifzadeh, S.; Govind, N.; Autschbach, J.; Neaton, J. B.; Baer, R.; Kronik, L. Quasiparticle Spectra from a Nonempirical Optimally Tuned Range-Separated Hybrid Density Functional. *Phys. Rev. Lett.* **2012**, *109*, 226405.

(74) Karolewski, A.; Kronik, L.; Kümmel, S. Using Optimally Tuned Range Separated Hybrid Functionals in Ground-State Calculations: Consequences and Caveats. *J. Chem. Phys.* **2013**, *138*, 204115.

(75) Tamblyn, I.; Refaely-Abramson, S.; Neaton, J. B.; Kronik, L. Simultaneous Determination of Structures, Vibrations, and Frontier Orbital Energies from a Self-Consistent Range-Separated Hybrid Functional. *J. Phys. Chem. Lett.* **2014**, *5*, 2734–2741.

(76) Brémond, É.; Pérez-Jiménez, Á. J.; Sancho-García, J. C.; Adamo, C. Range-Separated Hybrid Density Functionals Made Simple. *J. Chem. Phys.* **2019**, *150*, 201102.

(77) Brémond, É.; Pérez-Jiménez, Á. J.; Sancho-García, J. C.; Adamo, C. Range-Separated Hybrid and Double-Hybrid Density Functionals: A Quest for the Determination of the Range-Separation Parameter. *J. Chem. Phys.* **2020**, *152*, 244124.

(78) Feibelman, P. J. Energetics of Steps on Pt(111). *Phys. Rev. B* **1995**, *52*, 16845–16854.

(79) Füchsel, G.; Zhou, X.; Jiang, B.; Juaristi, J. I.; Alducin, M.; Guo, H.; Kroes, G.-J. Reactive and Nonreactive Scattering of HCl from Au(111): An Ab Initio Molecular Dynamics Study. *J. Phys. Chem. C* **2019**, *123*, 2287–2299.

(80) Gerrits, N.; Kroes, G.-J. Curious Mechanism of the Dissociative Chemisorption of Ammonia on Ru(0001). *J. Phys. Chem. C* **2019**, *123*, 28291–28300.

(81) Migliorini, D.; Nattino, F.; Tiwari, A. K.; Kroes, G.-J. HOD on Ni(111): Ab Initio Molecular Dynamics Prediction of Molecular Beam Experiments. *J. Chem. Phys.* **2018**, *149*, 244706.

(82) Füchsel, G.; del Cueto, M.; Díaz, C.; Kroes, G.-J. Enigmatic HCl + Au(111) Reaction: A Puzzle for Theory and Experiment. *J. Phys. Chem. C* **2016**, *120*, 25760–25779.

(83) Nattino, F.; Díaz, C.; Jackson, B.; Kroes, G.-J. Effect of Surface Motion on the Rotational Quadrupole Alignment Parameter of D_2 Reacting on Cu(111). *Phys. Rev. Lett.* **2012**, *108*, 236104.

(84) Ghassemi, E. N.; Wijzenbroek, M.; Somers, M. F.; Kroes, G.-J. Chemically Accurate Simulation of Dissociative Chemisorption of D_2 on Pt(111). *Chem. Phys. Lett.* **2017**, *683*, 329–335.

Supporting Figures

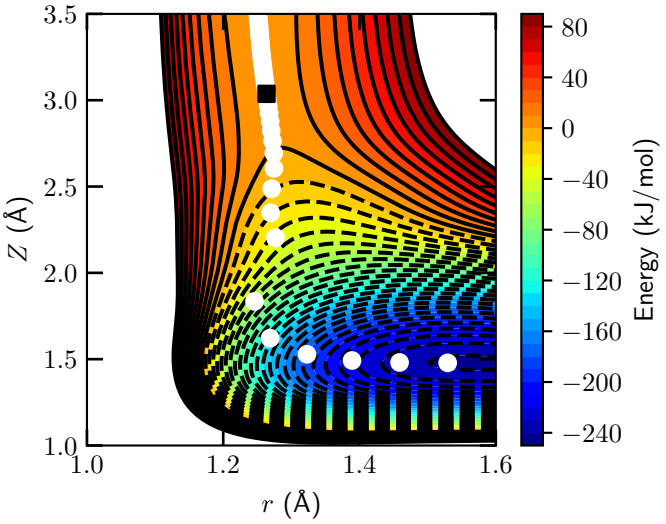

Figure S1: Elbow plot of the molecule-surface interaction energy of O_2 on Al(111) as a function of Z_{O_2} and r computed with the MS-RPBEl functional for the second parallel configuration at the fcc site (see Ref.[32]). Black contour lines are drawn at an interval of 10 kJ/mol between -250 and 100 kJ/mol. The white circles indicate the MEP in reduced dimensionality and the black square indicates the highest point along the MEP.

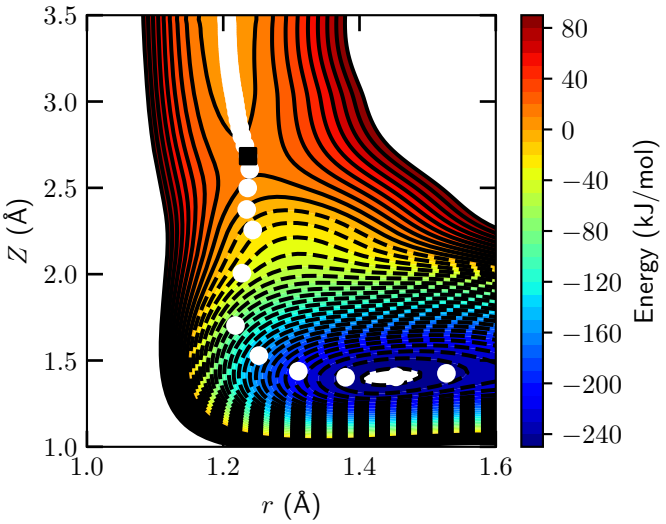

Figure S2: Elbow plot of the molecule-surface interaction energy of O_2 on Al(111) as a function of Z_{O_2} and r computed with the HSE03-1/3X functional for the second parallel configuration at the fcc site (see Ref.[32]). Black contour lines are drawn at an interval of 10 kJ/mol between -250 and 100 kJ/mol. The white circles indicate the MEP in reduced dimensionality and the black square indicates the highest point along the MEP.

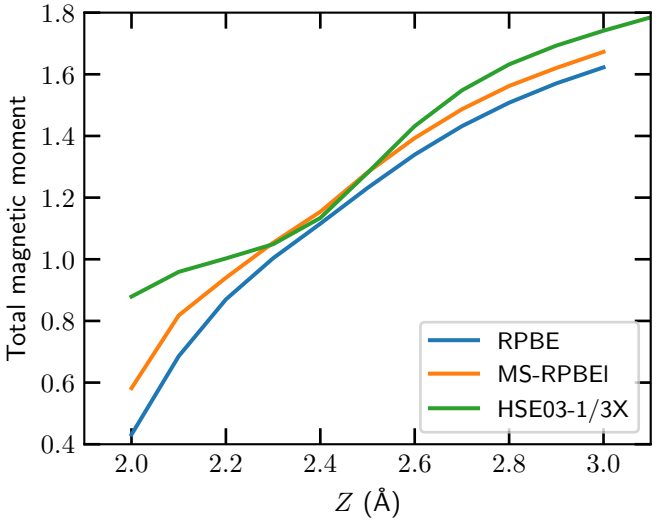

Figure S3: Total magnetic moment of the O_2 + Al(111) system as a function of Z_{O_2} for $r = 1.25$ Å and the fcc //3 configuration using several DFs.

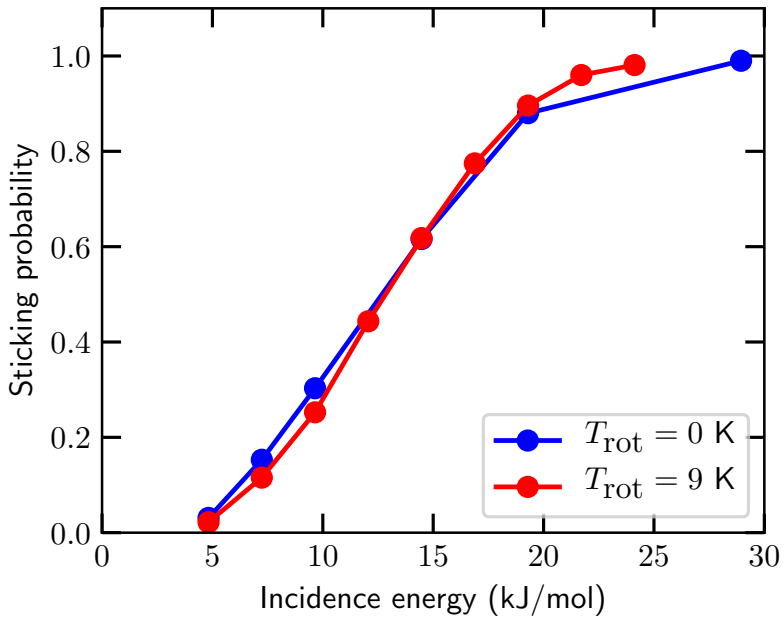

Figure S4: Sticking probability of O_2 on Al(111) as a function of translational energy for normal incidence. The blue circles indicate results for O_2 in the rovibrational ground state, whereas the red circles indicate results for a rovibrational state population according to $T_{\mathrm{vib}} = 300\,\mathrm{K}$ and $T_{\mathrm{rot}} = 9\,\mathrm{K}$.

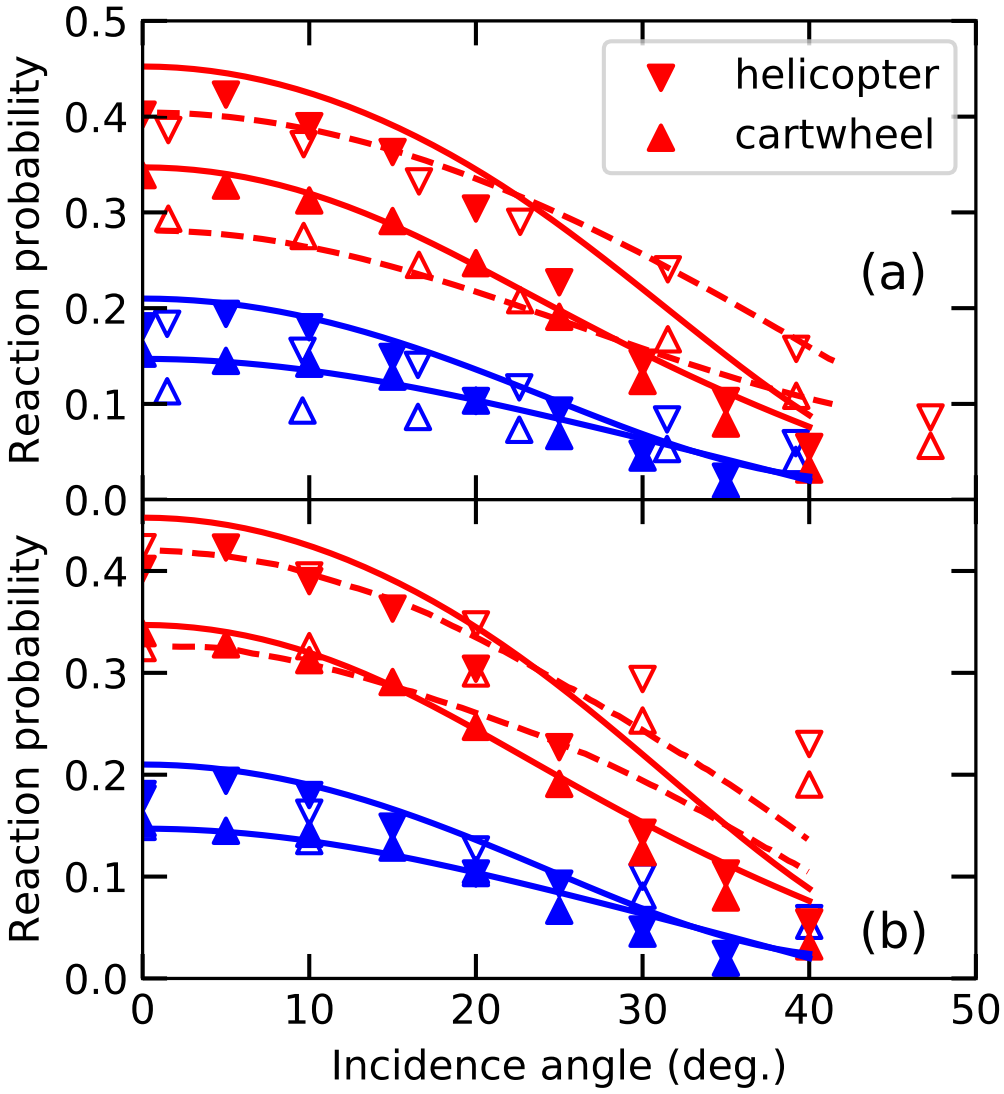

Figure S5: Sticking probability of O_2 ($\nu = 0, J = 2, K = 1$) on Al(111) as a function of incidence angle (degrees). (a) The solid symbols and lines indicate results obtained with the HSE03-1/3X DF for $E_\mathrm{i} = 8.2\,\mathrm{kJ/mol}$ (blue) and $E_\mathrm{i} = 11.1\,\mathrm{kJ/mol}$ (red). The open symbols and dashed lines indicate results from experiment[57] for $E_\mathrm{i} = 9.6\,\mathrm{kJ/mol}$ (blue) and $E_\mathrm{i} = 17.4\,\mathrm{kJ/mol}$ (red). The downward and upward pointing triangles correspond to the helicopter and cartwheel orientations, respectively. The lines correspond to results obtained with the assumption of normal energy scaling. (b) Same as panel a, but instead of experimental results, the results from a FPLEPS PES based on ECW data[32] for $E_\mathrm{i} = 14.5\,\mathrm{kJ/mol}$ (blue) and $E_\mathrm{i} = 22.2\,\mathrm{kJ/mol}$ (red) are shown. In both cases, the incidence energies in the calculations have been chosen such that similar reaction probabilities are obtained in the calculations as in the experiments.

Supporting Tables

Table S1: Work function values of several metal surfaces, which are taken from Ref.[34], except for the value for Pt(211), which was taken as the aforementioned value for Pt(111) plus the difference of calculated LDA values for Pt(211) and Pt(111) from Ref.[78].

Surface	Work function (eV)
Al(111)	4.32
Ni(111)	5.24
Au(111)	5.33
Ru(0001)	5.4
Cu(100)	4.73
Cu(111)	4.9
Pt(111)	5.91
Pt(211)	5.64

Table S2: Electron affinity values of several molecules, which are taken from Ref.[35] using semi-empirical composite theory with the G4 basis set, except for H_2O (CCSD(T) with a daug-cc-pVTZ basis set) and HCl (B97D3 DF with a aug-cc-pVTZ basis set), and except for CH_4, which was taken from Ref.[36].

Surface	Electron affinity (eV)
CH_4	-5.75
H_2	-3.155
O_2	0.463
HCl	-0.514
N_2	-1.982
NH_3	-0.897
H_2O	-0.181

Table S3: Minimum barrier heights and bulk lattice constants computed with different variations of the screened hybrid PBE DF, i.e., different exact exchange ratios and screening length parameters are employed. The barrier is taken to be at $Z = 2.8\,\text{Å}$, $r = 1.25\,\text{Å}$, and in the fcc //3 configuration. The row shown in bold face lists the functional used in the dynamics calculations, and presents the results obtained with it. The experimental value of the lattice constant is 4.032 Å[25].

DF	Exact exchange ratio	Screening length parameter (Å^{-1})	Bulk lattice constant (Å)	E_b (kJ/mol)
HSE06[4]	1/4	0.2	4.023	7.9
HSE06-1/3X	1/3	0.2	4.018	13.2
HSE06-1/2X	1/2	0.2	4.009	25.0
HSE03-1/3X	**1/3**	**0.3**	**4.022**	**12.8**
RSX-PBE0[77]	1/4	0.39	4.029	3.6
RSX-PBE0-1/3[77]	1/3	0.37	4.025	11.4

Table S4: Vibrational frequencies of the molecule at the reaction barrier geometries (see Table 2). Total zero point vibrational energies (ZPE) are also listed. Results are obtained from the HSE03-1/3X PES. The nomenclature of the different configurations is taken from Ref.[32].

		Vibrational mode (meV)						
site	orientation	1	2	3	4	5	6	ZPE (meV)
fcc	//1	138.4	18.5	8.2	5.9i	17.4i	87.2i	82.6
	//2	121.0	12.8	8.8	4.4i	15.7i	121.0i	71.3
	//3	89.5	14.9	4.1i	14.1i	18.8i	138.4i	52.2
	⊥	106.5	20.7	1.0	2.9i	20.6i	106.4i	64.1
top	//	115.6	14.9	5.9	5.9i	14.7i	115.6i	68.2
	⊥	131.2	21.8	1.1	0.9i	21.8i	131.2i	77.1
bridge	//	107.6	17.1	7.0	7.9i	15.6i	107.6i	65.9
	⊥	113.8	15.3	2.6	1.6i	15.9i	113.7i	65.9
gas phase		153.0	-	-	-	-	-	76.5

Table S5: Vibrational frequencies of the molecule at the reaction barrier geometries (see Table 2). Total zero point vibrational energies (ZPE) are also listed. Results are obtained from the MS-RPBEl PES. The nomenclature of the different configurations is taken from Ref.[32].

		Vibrational mode (meV)						
site	orientation	1	2	3	4	5	6	ZPE (meV)
fcc	//1	142.2	4.7	3.3	3.8i	5.8i	89.6i	75.1
	//2	118.9	3.9	2.6	3.9i	4.6i	118.9i	62.7
	//3	89.4	6.5	5.9	3.6i	5.6i	142.5i	50.9
	$\perp$	111.4	9.3	2.8	5.5i	9.1i	111.7i	61.8
top	//	113.3	8.3	0.9	4.3i	7.0i	113.3i	61.3
	$\perp$	115.9	8.1	0.1	2.0i	7.9i	115.9i	62.1
bridge	//	102.7	9.6	5.5	6.0i	8.6i	102.7i	58.9
	$\perp$	115.6	6.4	0.6	1.4i	6.9i	115.5i	61.3
gas phase		146.6	-	-	-	-	-	73.3

Table S6: Barrier height (in kJ/mol) of O_2 on Al(111) obtained from the HSE03-1/3X CRP PES and HSE03-1/3X@RPBE calculations. The nomenclature of the different configurations is taken from Ref.[32].

site	orientation	$E_{\mathrm{b,HSE03\text{-}1/3X}}$	$E_{\mathrm{b,HSE03\text{-}1/3X@RPBE}}$
fcc	//1	12.3	11.5
	//2	11.4	10.3
	//3	12.3	11.4
	$\perp$	26.9	30.1
top	//	22.2	21.5
	$\perp$	26.8	29.0
bridge	//	29.4	31.1
	$\perp$	19.4	22.7

Table S7: Barrier heights (in kJ/mol) obtained self-consistently and non-self-consistently for three of the five difficult systems (see Figure 1). All calculations are performed for a 2×2 supercell, $8 \times 8 \times 1$ k-point grid and a kinetic energy cut-off of 400 eV.

System	DF	$E_{\mathrm{b,DF}}$	$E_{\mathrm{b,HSE03\text{-}1/3X@DF}}$	$E_{\mathrm{b,HSE03\text{-}1/2X@DF}}$	$E_{\mathrm{b,PBE}}$	$W - E_{\mathrm{ea}}$ (eV)	Excess charge (e^-)
Al(111) + O_2	RPBE	0.1	12.5	29.9	-	3.857	0.332
Au(111) + HCl[79]	RPBE-vdW-DF1	85.1	106.2	122.9	72.9	5.844	0.318
Ru(0001) + NH_3[80]	RPBE-vdW-DF1	68.6	53.8	60.6	38.7	6.297	0.348

Table S8: Excess charge at the molecule for the TS compared to a neutral molecule for several systems obtained with the Bader charge decomposition scheme.

System	DF	$W - E_{\mathrm{ea}}$ (eV)	Excess charge (e^-)
Al(111) + O_2	HSE03-1/3X	3.857	0.332
Ni(111) + H_2O[81]	SRP32-vdW-DF1	5.421	0.472
Au(111) + HCl[82]	RPBE	5.844	0.348
Ru(0001) + NH_3[80]	SRP32-vdW-DF1	6.297	0.348
Cu(111) + H_2[83]	SRP48	8.055	0.229
Pt(111) + H_2[84]	PBEa57-vdW-DF2	9.065	-0.047
Ni(111) + CH_4[7]	SRP32-vdW-DF1	10.99	0.241